Applied Physics A (2022) 128:531
https://doi.org/10.1007/s00339-022-05678-8

Applied Physics A
Materials Science & Processing

Effects of Bi_2Te_3 doping on the thermoelectric properties of Cu_2Se alloys

Rui Ma[1] · Delin Yang[1,2] · Zengguo Tian[1] · Hongzhang Song[1] · Yingjiu Zhang[1]

Received: 6 April 2022 / Accepted: 8 May 2022 / Published online: 27 May 2022

Abstract
Cu_2Se and Bi_2Te_3 nano-powders prepared by the hydrothermal method were mixed and hot-pressed according to the molar ratio $Cu_2Se + x$ mol% Bi_2Te_3 ($x = 0, 1, 2, 3$). Bi_2Te_3 doping as the second phase can influence the microstructure of Cu_2Se greatly, increase the carrier mobility and concentration, and reduce the resistivity significantly. The power factor increases by 17–42% compared with the pure sample. However, the total thermal conductivity increases further, which is not our expectation. Finally, the dimensionless thermoelectric figure of merit ZT is not well optimized.

Keywords Thermoelectric materials · Cu_2Se · Bi_2Te_3 · Second-phase compound

1 Introduction

In recent years, the extensive use of fossil fuels has caused the depletion danger and a series of environmental problems such as air pollution, water pollution and the greenhouse effect. Environmental and energy problems need to be solved urgently [1, 2]. Thermoelectric materials can realize the mutual conversion of thermal energy and electric energy with the advantages of environmental friendliness, long service time, and noiseless operation. They are also expected to be one of the most promising materials for solving current environmental and energy problems. Of course, the low energy conversion efficiency affects the application range of thermoelectric materials. However, they are still in a state of needing to improve the thermoelectric performance to achieve relatively stable and high thermoelectric values.

After the 1960s, the research on thermoelectric materials was focused on several typical material systems such as Bi_2Te_3 [3], PbTe [4], Si/Ge [5] alloys. Bi_2Te_3 is represented in the room temperature region (< 400 K) [6, 7], PbTe, $SbSe_3$, GeTe in the medium temperature region (600–900 K) [8–10], and Si/Ge in the high temperature region (> 900 K) [11, 12]. All of them have been used in some specific fields. However, in these materials, such as Bi, Pb, and Te are usually expensive or scarce elements. Most importantly, they contain toxic heavy metals, which can easily cause bad environment pollution problems. So it is necessary to find efficient and pollution-free thermoelectric materials. Cu_2Se is a promising thermoelectric material that can replace PbTe. It is non-toxic and non-polluting [13–15]. The performance of thermoelectric materials is determined by the dimensionless thermoelectric figure of merit ZT,

$$\mathrm{ZT} = \frac{S^2}{\rho\kappa}T = \frac{\mathrm{PF}}{\kappa}T = \frac{\mathrm{PF}}{\kappa_e + \kappa_l}T.$$

S is the Seebeck coefficient, ρ is the resistivity, T is the absolute temperature, and κ is the total thermal conductivity, including electronic thermal conductivity (κ_e) and lattice thermal conductivity (κ_l). The three parameters S, ρ, and κ are coupled with each other [16]. It is difficult to improve the three parameters at the same time [17]. Among them, the power factor (PF) reflects the electrical transport performance, and κ reflects the thermal transport performance. Relatively speaking, it is relatively easy to control the power factor (PF) or the thermal conductivity (κ) individually. There are various methods to improve the power factor, such as element doping [18, 19], multi-band convergence [20], etc. These methods mainly achieve the purpose of improving the power factor

✉ Hongzhang Song
hzsong@zzu.edu.cn

✉ Yingjiu Zhang
zhangyj2006@zzu.edu.cn

[1] Key Laboratory of Material Physics of Ministry of Education, School of Physics and Microelectrons, Zhengzhou University, Zhengzhou 450001, China

[2] Huanghe Science and Technology College, Zhengzhou 450006, China

by optimizing the carrier transport characteristics. Methods of optimizing thermal conductivity include secondary phase recombination [17, 21], pore engineering [17, 22], nano-engineering [23, 24], etc. These methods are mainly accomplished by enhancing phonon scattering.

In the previous research of our group, the nanostructure engineering and element doping in Cu_2Se were ever investigated. For example, the doping of alkali metals (Na, K, Li) could introduce some micropores to reduce the lattice thermal conductivity [25–27], where the highest ZT value of $Cu_{1.98}Li_{0.02}Se$ reached 2.14 at 973 K [27]. The doping of heavy metals (Pb, Hg, Ni) was more complicated [28–30]. For example, when doping Pb, it was mainly caused by ionized impurity scattering, point defects, and the reduction of hole concentration. Although the electrical transport performance of Cu_2PbSe decreases, it also reduced the thermal conductivity, which ultimately increases the thermal transport performance. Therefore, the optimal value of $Cu_{1.95}Pb_{0.015}Se$ at 873 K reached 1.5 [28].

Many literatures reported that the thermoelectric figure of merit (ZT) could be improved by the second-phase composite method. For example, carbon-based materials were used as second-phase composites. In carbon-dot-doped Cu_2Se, its thermal conductivity was depressed greatly due to enhanced phonon scattering, and its ZT value reached 1.98 at 973 K [31]. In graphene doped Cu_2Se, its thermal conductivity of was reduced greatly by up to 50% compared with the carbon-free sample. When the mass ratio of doping was 0.15%, the ZT value could be as high as 2.4 [32]. In the Cu_2Se/CNTs hybrid material, CNTs were dispersed as the second phase, in which phonons were scattered in Cu_2Se to inhibit heat conduction. The Cu-embedded CNTs reduced the carrier concentration by providing Cu to absorb holes in Cu_2Se [33–35]. In the GeTe matrix, dispersed Bi_2Te_3 on the basis of Pb doping could reduce the carrier concentration. It could also make the valence band closer [36]. As a result, the number of point defects had increased dramatically, and collectively reduced thermal conductivity from different angles. Its thermoelectric performance had been improved greatly.

In Bi_2Te_3 matrix, Cu_2Se was doped as the second phase, which could optimize the phonon and carrier transport properties at the same time. The dimensionless thermoelectric figure of merit ZT increased by 45% [37]. At present, there was no literature report on doping Bi_2Te_3 in Cu_2Se. Therefore, in this paper, the influence of Bi_2Te_3 as the second phase on the thermoelectric properties of Cu_2Se alloys was studied.

2 Experimental

In this work, Bi_2Te_3 and Cu_2Se nano-powders were synthesized by the hydrothermal synthesis method. Bi_2Te_3 was synthesized with analytical grade compound $BiCl_3$ (AR), Te powder (99.9%), NaOH (AR), SDBS (AR) and reducing agent $NaBH_4$ (AR) as precursors. The precursors were placed in a Teflon-lined autoclave containing about 120 ml of deionized water, stirred on a stirring table with a rotating speed of 1000 rpm for 0.5 h. After sealing, it was obtained after reaction for 24 h at 443 K. In order to remove impurities, deionized water, anhydrous alcohol, and propanol filter were used for three times to clean the powders, and it was dried at 333 K in a vacuum chamber for 3 h. The analytical grade compound $CuCl_2{\cdot}2H_2O$ (99.99%) and SeO_2 (99.99%) were used as precursors to synthesize Cu_2Se. The precursors were placed in a Teflon-lined autoclave containing about 120 ml of deionized water, stirred on a stirring table with a rotating speed of 1000 rpm for 1.5 h. After stirring, about 5 ml reductant($N_2H_4{\cdot}2H_2O$) was added to the autoclave. To remove the by-products of the reaction, deionized water and alcohol filter were used for three times to clean the powders. The filtered powder was dried in a vacuum chamber for 4 h at 373 K. Finally, the two hydrothermal synthesized nano-powders were mixed and ground in an agate mortar according to the proportion of $Cu_2Se + x$ mol% Bi_2Te_3 ($x = 0$, 1, 2, 3) for 30 min, and then were hot-pressed at 1073 K, 65 MPa for 15 min into blocks with a diameter of 10 or 12.5 mm.

The prepared samples were subjected to room temperature powder analysis using an X-ray diffraction analyzer (XRD, PANalytical, Netherlands) with Cu-$K_\alpha$radiation to determine the composition of the samples. The microstructure at the fracture of the sample was observed by scanning electron microscope (SEM, JSM-6700F, Japan). The Seebeck coefficient and resistivity measurements were carried out using a LSR system (Linseis, Germany) under the protection of helium gas, and their test temperature range was from 298 to 923 K. Thermal conductivity (κ) was measured by STAPT 1650 (Linseis, Germany) and the LFA 457 system (Netzsch, Germany) to obtain the heat capacity C_p and the thermal diffusivity α, respectively. It was calculated using $\kappa = \alpha D C_p$, where D was the sample density.

3 Results and discussion

Figure 1 shows the room temperature XRD patterns for $Cu_2Se + x$ mol% Bi_2Te_3 ($x = 0$, 1, 2, 3) samples. Cu_2Se has a relatively complex atomic arrangement, in which Se atoms can form relatively stable face-centered cubic sublattices network structure, which maintains good electrical transport properties [38, 39]. The Cu ions are distributed in different gap positions for free migration. From the XRD patterns, within the error range of the detection instrument, when the doping amount is less than 3%, there is no impurity peak, and the existence of Bi_2Te_3 is not found. But with the increase of the doping amount, when the doping amount is greater than 3%, there is spurious peaks. By comparing the

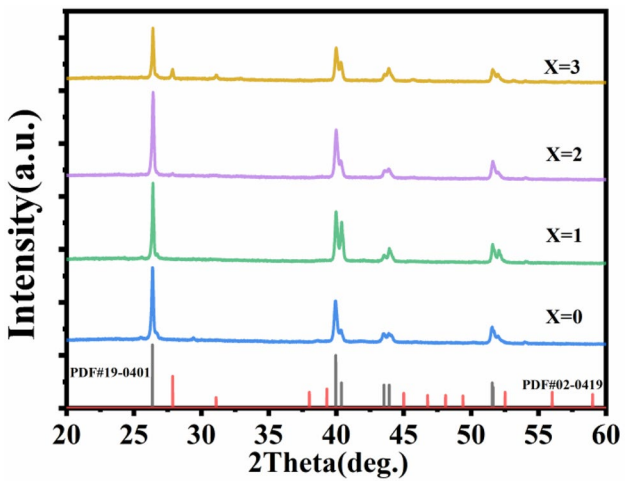

Fig.1 XRD patterns for the $Cu_2Se + x$ mol% Bi_2Te_3($x = 0, 1, 2, 3$)

PDF cards, it is found that the spurious peaks are the peaks of Bi.

Figure 2 shows the SEM images of the sample fracture. For the pure Cu_2Se sample in Fig. 2(a), the sample exists laminar structure, with more micro-holes. The formation of micro-holes is mainly explained by the following two kinds of explanation. One is that, according to the literature of Ge et al. [40], micro-holes are left by the volatilization of Na and Se elements during the high temperature preparation process. Another is in the work of Hu et al. [27], which illustrates that the number of nanopores decreases or even disappears with the decrease of hot-pressure sintering temperature. During the sintering process at high temperature and pressure the material will form liquid or gas phase, and the shrinkage rate of liquid and solid phase is different. Thus the liquid deviation phenomenon will occur leading to the formation of pores [41]. From the figures (b), (c), and (d), the samples all have obvious layered structures. With the increase of doping amount, it can be observed that the micro-holes are getting less and less. The reason may be that the nanoscale Bi_2Te_3 act as a sintering aid in the hot pressing link, which promotes the sintering to the extent that the holes become less and less. This is consistent with their densities, which are 6.061, 6.191, 6.469 and 6.589 g/cm^3, respectively. From the SEM images, it can be seen that the grain size in the crystal has locally become larger. As the grain size increases, the free path of carriers and phonons increases. It is less easy to scattering. It contributes to the increase of carrier mobility. The resistivity decreases and the thermal conductivity increases.

Due to the special structure of Cu_2Se, it has the characteristic of "phonon-liquid electron-crystal" [42, 43]. It not only keeps the characteristics of solid crystal, but also has the characteristics of liquid-like sublattice melting of Cu^+ [44]. The secondary phase change process is at about 350 K, Cu_2Se from α-phase to β-phase, and there is a mutation

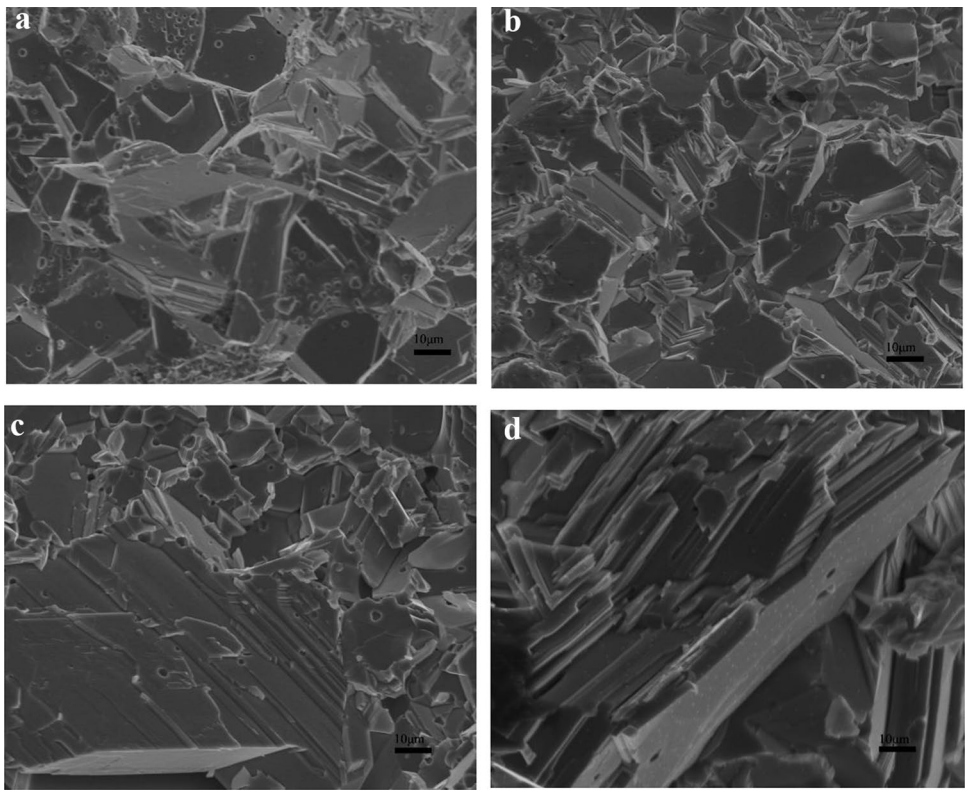

Fig. 2 Fracture SEM images of $Cu_2Se + x$ mol% Bi_2Te_3 ($x = 0$, 1, 2, 3) samples **a** $x = 0$ **b** $x = 1$ **c** $x = 2$ **d** $x = 3$

point. During this transformation, the cubic sublattice of Se atoms remains almost unchanged, and the arrangement of Cu ions embedded in the Se sublattice would change with the increase of temperature, which ends up in a random and disordered distribution in the cubic sublattice of Se [38]. In this process, the crystal structure of Cu_2Se changes from monoclinic layered structure to cubic crystal structure, which is also irreversible. This secondary structure phase transition in Cu_2Se can lead to violent fluctuations in the density, carrier concentration and structure of the material. This is the reason for appearance of peaks at about 350 K in Fig. 3.

From the change of the Seebeck coefficient with temperature in Fig. 3(a), it can be seen that the Seebeck coefficient decreases significantly with the increase of doping amount. Due to doping *n*-type Bi_2Te_3, the crystal interior is no longer a single carrier. Under the intrinsic thermal excitation, it can lead to mixed conduction of electrons and holes, which deteriorates the Seebeck coefficient of the material. In addition, the increase of carrier concentration can also reduce the Seebeck coefficient. This phenomenon is different from the reference [37]. From the Fig. 3(b), the resistivity has a huge decrease through the doping of Bi_2Te_3. On side, Bi_2Te_3 is a typical narrow-band semiconductor material with excellent thermoelectric properties at room temperature [45]. The electronegativity difference between Bi atoms and Te atoms is very small, and they have relatively high carrier mobility. They have excellent electrical transport properties. The increase in carrier concertation is mainly due to the introduction of Bi^{3+}, which injects a large number of electrons. The other side of the shield, according to the previous SEM images. With the increase of doping amount, the micro-holes become less and less and the grain size becomes larger and larger, the carrier mobility increase. Therefore, doping a small amount of Bi_2Te_3 nano-powder can greatly improve the carrier mobility and reduce the resistivity. Compared with undoped samples, the resistivity decreases by two to five times. From the Fig. 3(c), it can be calculated from the formula $PF = S^2 * T/\rho$, where ρ is the resistivity, T is the temperature. The calculated power factor as a function of temperature shows that the doping with an amount of Bi_2Te_3 leads to a significant improvement in the electrical transport performance of Cu_2Se, mainly due to the increase in carrier mobility and concentration. Compared with undoped samples, power factor increases by 17–42%.

From Fig. 4, the thermal conductivity between 473 and 873 K was tested. The thermal conductivity is determined by the lattice thermal conductivity, the electron thermal conductivity and bipolar diffusion thermal conductivity. The electronic thermal conductivity can be calculated according to Wiedemann–Franz law. The lattice thermal conductivity and bipolar diffusion thermal conductivity can be obtained by $\kappa_l + \kappa_b = \kappa - \kappa_e$. The lattice thermal conductivity, bipolar diffusion thermal conductivity, and the electronic thermal conductivity as a function of temperature are thus obtained

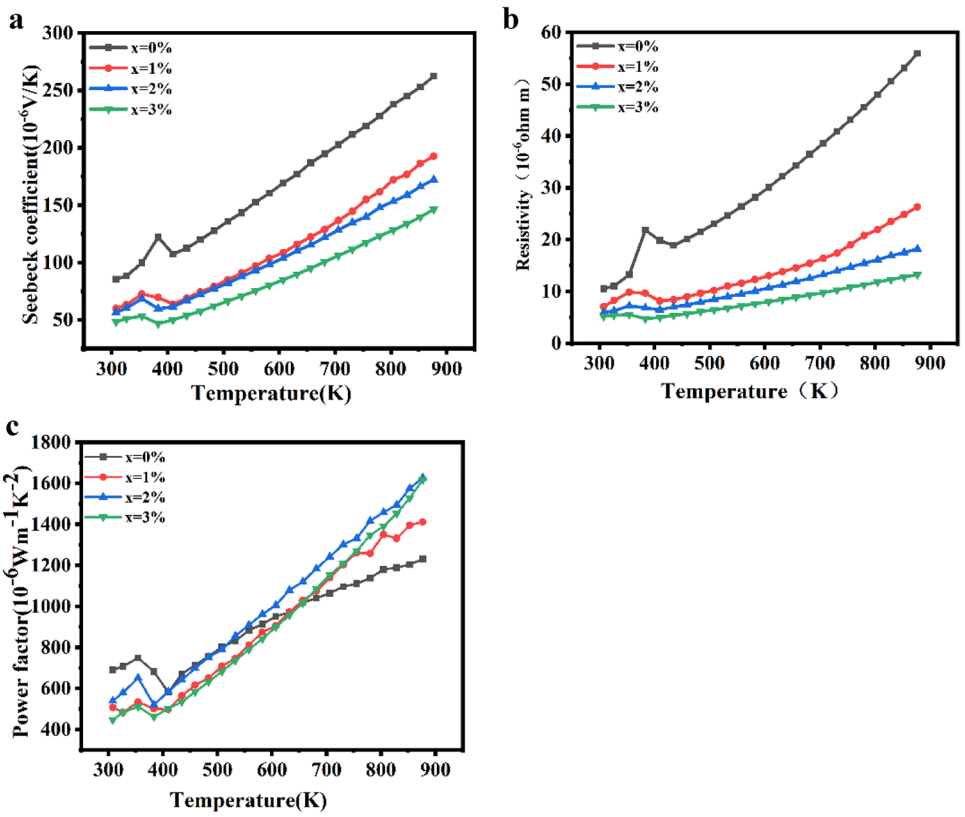

Fig. 3 Schematic diagram of the electrical transport properties of $Cu_2Se + x$ mol% Bi_2Te_3 ($x = 0$, 1, 2, 3) as a function of temperature **a** Seebeck coefficient **b** Resistivity **c** Power factor

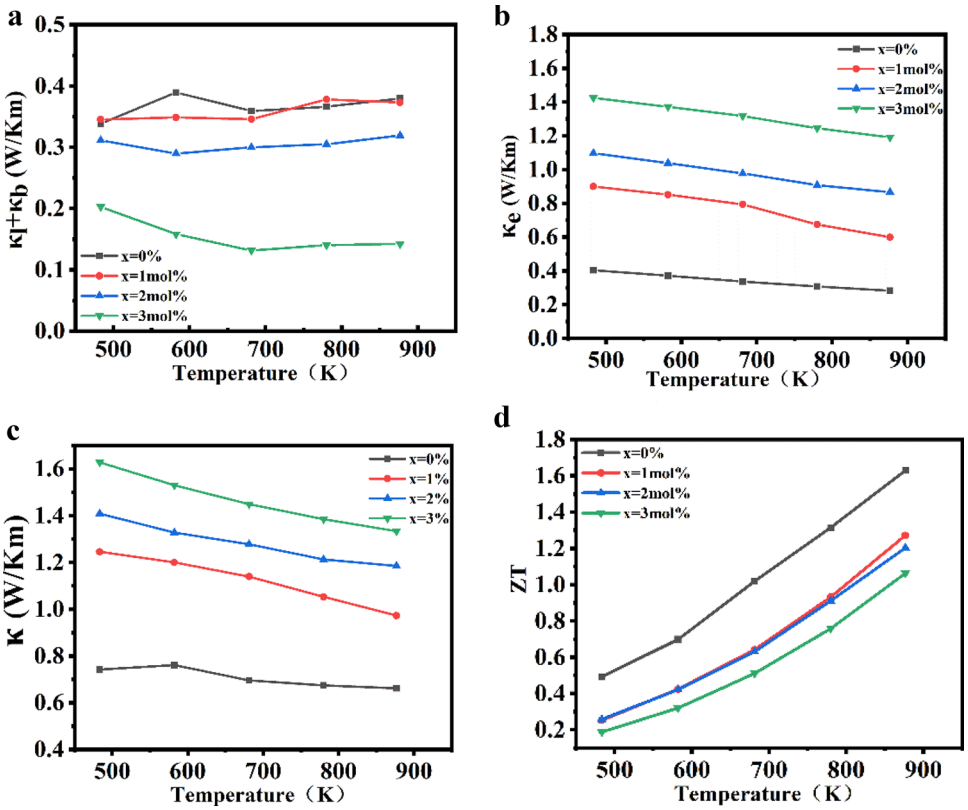

Fig. 4 Schematic diagram of thermal transport properties of Cu_2Se+x mol% Bi_2Te_3 ($x=0$, 1, 2, 3) as a function of temperature **a** Lattice thermal conductivity and bipolar diffusion thermal conductivity ($\kappa_l + \kappa_b$) **b** Electron thermal conductivity (κ_e) **c** The total thermal conductivity (κ) **d** ZT value

schematically. From Fig. 4(a), it can be seen that the lattice thermal conductivity is decreased with the increase in the amount of doped Bi_2Te_3. This is consistent with the references. Chen et al. [37] explained that in the synthesis process, Cu_2Se additive reacted with the Bi_2Te_3 matrix. The decrease of the lattice thermal conductivity was attributed to strong phonon scattering by the hierarchical structure, including Te defect area, Cu_7Te_5 secondary phase inclusions and phase boundaries. In this work, the reduction of the lattice thermal conductivity is also attributed to phonon scattering by the phase boundary caused by doping Bi_2Te_3. However, in Fig. 4(b), the electronic thermal conductivity has been improved greatly, which is consistent with the reduction in the Seebeck coefficient and resistivity in the previous discussion caused by the increase in carrier concentration. Figure 4(c), the final thermal conductivity is greatly increased. On the one hand, the reason is the introduction of Bi^{3+} injects a large number of electrons to increase electron concentration. On the other hand, during the transport process, the hole–electron pairs generated by the intrinsic excitation compound with a certain probability and give off heat greater than or equal to the forbidden band width of the sample, resulting in an additional contribution to heat conduction. Therefore, the thermal conductivity is greatly improved. Although, the doping of Bi_2Te_3 can indeed reduce the lattice thermal conductivity to a certain extent, and the effect is relatively obvious. From the diagram, the electron thermal conductivity plays a major role. This is inconsistent with our expectations or any reported references [37]. The reason of this abnormal phenomenon may be that the doping amount is too big, and that the sintering aid effect exceeds the dispersion additive effect. For example, the doping amount x is <0.03 in the Bi–Se co-doped Cu_2S [46].

Figure 4(d) shows the changes of ZT value with temperature. Finally, the ZT value of the pure sample reaches 1.6 at 873 K, due to its micro-hole structure. Compared with the reported pure samples with the nominal component Cu_2Se, the dimensionless thermoelectric figure of merit ZT in this work is higher. It is a pity that although power factor is improved, thermal conductivity increases more. Thus, the thermoelectric performance of Bi_2Te_3-doped samples is not optimized. For example, the ZT value of the 1% doping sample only reach 1.2 at 873 K.

4 Conclusion

In summary, pure Bi_2Te_3 and Cu_2Se nano-powders were prepared by hydrothermal synthesis. Doped with Cu_2Se+x mol% Bi_2Te_3 ($x=0$, 1, 2, 3), they were pressed into blocks by the hot-press sintering technique. The Bi_2Te_3, which was introduced into Cu_2Se as a second phase, can greatly reduce the resistivity and improve the power factor compared with pure Cu_2Se samples. At the same time, the lattice thermal

conductivity can also be effectively reduced. But the electronic thermal conductivity is greatly increased, the final thermal conductivity is not effectively reduced. The significance of this work is that it is possible to consider different thermoelectric materials for second-phase compounding, which to a certain extent can modify the interface and affect the changes in resistivity and thermal conductivity [36, 37, 47, 48]. The second-phase compounding could be also an effective approach in improving the thermoelectric properties of thermoelectric materials [49–51].

Declarations

Conflict of interest On behalf of all authors, the corresponding author states that there are no conflicts of interests.

References

1. Y. Wang, Y.V. Lim, S. Huang, M. Ding, D. Kong, Y. Pei, T. Xu, Y. Shi, X. Li, H.Y. Yang, Enhanced sodium storage kinetics by volume regulation and surface engineering via rationally designed hierarchical porous FeP@C/rGO. Nanoscale **12**, 4341–4351 (2020)
2. D. Wu, Z. Zhao, W. Lu, L. Rogée, L. Zeng, P. Lin, Z. Shi, Y. Tian, X. Li, Y.H. Tsang, Highly sensitive solar-blind deep ultraviolet photodetector based on graphene/$PtSe_2$/β-Ga_2O_3 2D/3D Schottky junction with ultrafast speed. Nano Res. **14**, 1973–1979 (2021)
3. S. Bano, A. Kumar, B. Govind, A.H. Khan, A. Ashok, D. Misra, Room temperature Bi_2Te_3-based thermoelectric materials with high performance. J. Mater. Sci. Mater. Electron. **31**, 8607–8617 (2020)
4. Y. Xiao, H. Wu, J. Cui, D. Wang, L. Fu, Y. Zhang, Y. Chen, J. He, S.J. Pennycook, L.D. Zhao, Realizing high performance n-type PbTe by synergistically optimizing effective mass and carrier mobility and suppressing bipolar thermal conductivity. Energy Environ. Sci. **11**, 2486–2495 (2018)
5. Omprakash, M., Singh, S., Hirata, K., Kuga, K., Harish, S., Shimomura, M., Adachi, M., Yamamoto, Y., Matsunami, M. and Takeuchi, T. Synergetic enhancement of power factor and suppression of lattice thermal conductivity via electronic structure modification and nanostructuring on Ni and B co-doped p-type Si-Ge alloy. arXiv preprint arXiv:2107.13778. (2021)
6. B. Zhu, X. Liu, Q. Wang, Y. Qiu, Z. Shu, Z. Guo, Y. Tong, J. Cui, M. Gu, J. He, Realizing record high performance in n-type Bi_2Te_3-based thermoelectric materials. Energy Environ. Sci. **13**, 2106–2114 (2020)
7. F. Wu, Q. He, M. Tang, H. Song, Thermoelectric properties of Tl and I dual-doped Bi_2Te_3-based alloys. Int. J. Mod. Phys. B **32**, 1850123 (2018)
8. D. An, S. Chen, Z. Lu, R. Li, W. Chen, W. Fan, W. Wang, Y. Wu, Low thermal conductivity and optimized thermoelectric properties of p-type Te–Sb_2Se_3: synergistic effect of doping and defect engineering. ACS Appl. Mater. Interfaces. **11**, 27788–27797 (2019)
9. J. Shuai, Y. Sun, X. Tan, T. Mori, Manipulating the Ge vacancies and Ge precipitates through Cr doping for realizing the high-performance GeTe thermoelectric material. Small **16**, 1906921 (2020)
10. J.P. Heremans, V. Jovovic, E.S. Toberer, A. Saramat, K. Kurosaki, A. Charoenphakdee, S. Yamanaka, G.J. Snyder, Enhancement of thermoelectric efficiency in PbTe by distortion of the electronic density of states. Science **321**, 554–557 (2008)
11. O. Muthusamy, S. Singh, K. Hirata, K. Kuga, S.K. Harish, M. Shimomura, M. Adachi, Y. Yamamoto, M. Matsunami, T. Takeuchi, Synergetic enhancement of the power factor and suppression of lattice thermal conductivity via electronic structure modification and nanostructuring on a Ni-and B-codoped p-type Si–Ge alloy for thermoelectric application. ACS Appl. Electron. Mater. **3**, 5621–5631 (2021)
12. R. Basu, A. Singh, High temperature Si–Ge alloy towards thermoelectric applications: a comprehensive review. Mater. Today Phys. **21**, 100468 (2021)
13. W.-D. Liu, L. Yang, Z.-G. Chen, Cu_2Se thermoelectrics: property, methodology, and device. Nano Today **35**, 100938 (2020)
14. Y. Qin, L. Yang, J. Wei, S. Yang, M. Zhang, X. Wang, F. Yang, Doping effect on Cu_2Se thermoelectric performance: a review. Materials **13**, 5704 (2020)
15. L. Xue, C. Fang, W. Shen, M. Shen, W. Ji, Y. Zhang, Z. Zhang, X. Jia, High pressure synthesis and thermoelectric performances of Cu_2Se compounds. Phys. Lett. A **383**, 125917 (2019)
16. W.D. Liu, L. Yang, Z.G. Chen, J. Zou, Promising and eco-friendly Cu_2X-based thermoelectric materials: progress and applications. Adv. Mater. **32**, 1905703 (2020)
17. L. Yang, Z.-G. Chen, G. Han, M. Hong, Y. Zou, J. Zou, High-performance thermoelectric Cu_2Se nanoplates through nanostructure engineering. Nano Energy **16**, 367–374 (2015)
18. L. Yang, Z.G. Chen, G. Han, M. Hong, L. Huang, J. Zou, Te-Doped Cu_2Se nanoplates with a high average thermoelectric figure of merit. J. Mater. Chem. A. **4**, 9213–9219 (2016). https://doi.org/10.1039/C6TA02998A
19. F. Liu, Z. Gong, M. Huang, W. Ao, Y. Li, J. Li, Enhanced thermoelectric properties of β-Cu_2Se by incorporating $CuGaSe_2$. J. Alloy. Compd. **688**, 521–526 (2016)
20. J. Mao, W. Liu, Z. Ren, Carrier distribution in multi-band materials and its effect on thermoelectric properties. J. Materiomics **2**, 203–211 (2016)
21. L. Zhao, S.M.K.N. Islam, J. Wang, D.L. Cortie, X. Wang, Z. Cheng, J. Wang, N. Ye, S. Dou, X. Shi, Significant enhancement of figure-of-merit in carbon-reinforced Cu_2Se nanocrystalline solids. Nano Energy **41**, 164–171 (2017)
22. J. Zhang, T. Zhu, C. Zhang, Y. Yan, G. Tan, W. Liu, X. Su, X. Tang, In-situ formed nano-pore induced by ultrasonication boosts the thermoelectric performance of Cu_2Se compounds. J. Alloy. Compd. **881**, 160639 (2021)
23. F. Gao, S. Leng, Z. Zhu, X. Li, X. Hu, H. Song, Preparation and thermoelectric properties of Cu_2Se hot-pressed from hydrothermal synthesis nanopowders. J. Electron. Mater. **47**, 2454–2460 (2018)
24. F. Wu, H. Song, J. Jia, F. Gao, Y. Zhang, X. Hu, Thermoelectric properties of Ce-doped n-type $Ce_xBi_{2-x}Te_{2.7}Se_{0.3}$ nanocomposites. Phys. Status Solidi A **210**, 1183–1189 (2013)
25. Z. Zhu, Y. Zhang, H. Song, X.-J. Li, High thermoelectric performance and low thermal conductivity in $Cu_{2-x}Na_xSe$ bulk materials with micro-pores. Appl. Phys. A **125**, 572 (2019)
26. Z. Zhu, Y. Zhang, H. Song, X.-J. Li, Enhancement of thermoelectric performance of Cu_2Se by K doping. Appl. Phys. A **124**, 871 (2018)
27. Q. Hu, Z. Zhu, Y. Zhang, X.-J. Li, H. Song, Y. Zhang, Remarkably high thermoelectric performance of $Cu_{2-x}Li_xSe$ bulks with nanopores. J. Mater. Chem. A **6**, 23417–23424 (2018)
28. Z. Zhu, Y. Zhang, H. Song, X.J. Li, Enhancement of thermoelectric performance of $Cu_{1.98}Se$ by Pb doping. Appl. Phys. A **124**, 747 (2018)

29. E. Li, S. Wang, Z. Zhu, R. Cao, X. Hu, H. Song, Enhanced thermoelectric properties of Hg-doped Cu_2Se. Int. J. Mod. Phys. B **32**, 1850087 (2018)
30. F. Gao, X. Du, F. Wu, X. Li, X. Hu, H. Song, Thermoelectric properties of $Cu_2Se/xNi_{0.85}Se$ hot-pressed from hydrothermal synthesis nanopowders. Mod. Phys. Lett. B **31**, 1750093 (2017)
31. Q. Hu, Y. Zhang, Y. Zhang, X.J. Li, H. Song, High thermoelectric performance in Cu_2Se/CDs hybrid materials. J. Alloy. Compd. **813**, 152204 (2019)
32. M. Li, D.L. Cortie, J. Liu, D. Yu, S.M.K.N. Islam, L. Zhao, D.R. Mitchell, R.A. Mole, M.B. Cortie, S. Dou, Ultra-high thermoelectric performance in graphene incorporated Cu_2Se: role of mismatching phonon modes. Nano Energy **53**, 993–1002 (2018)
33. R. Nunna, P. Qiu, M. Yin, H. Chen, R. Hanus, Q. Song, T. Zhang, M.-Y. Chou, M.T. Agne, J. He, Ultrahigh thermoelectric performance in Cu_2Se-based hybrid materials with highly dispersed molecular CNTs. Energy Environ. Sci. **10**, 1928–1935 (2017)
34. R. Cao, Z. Zhu, X.-J. Li, X. Hu, H. Song, Enhanced thermoelectric properties of the Lu-doped and CNT-dispersed Bi_2Te_3 alloy. Appl. Phys. A **125**, 126 (2019)
35. X. Li, J. Fu, Y. Sun, M. Sun, S. Cheng, K. Chen, X. Yang, Q. Lou, T. Xu, Y. Shang, Design and understanding of core/branch-structured VS_2 nanosheets@ CNTs as high-performance anode materials for lithium-ion batteries. Nanoscale **11**, 13343–13353 (2019)
36. D. Wu, L.-D. Zhao, S. Hao, Q. Jiang, F. Zheng, J.W. Doak, H. Wu, H. Chi, Y. Gelbstein, C. Uher, Origin of the high performance in GeTe-based thermoelectric materials upon Bi_2Te_3 doping. J. Am. Chem. Soc. **136**, 11412–11419 (2014)
37. J. Chen, D. Bao, Q. Sun, W.-D. Liu, C. Liu, J. Tang, L. Yang, D. Zhou, M.S. Dargusch, Z.-G. Chen, Simultaneously optimized thermoelectric performance of n-type Cu_2Se alloyed Bi_2Te_3. J. Solid State Chem. **296**, 121987 (2021)
38. P. Lu, H. Liu, X. Yuan, F. Xu, X. Shi, K. Zhao, W. Qiu, W. Zhang, L. Chen, Multiformity and fluctuation of Cu ordering in Cu_2Se thermoelectric materials. J. Mater. Chem. A **3**, 6901–6908 (2015)
39. F. Rong, Y. Bai, T. Chen, W. Zheng, Chemical synthesis of Cu_2Se nanoparticles at room temperature. Mater. Res. Bull. **247**, 92–95 (2012)
40. Z.H. Ge, X. Liu, D. Feng, J. Lin, J. He, High-performance thermoelectricity in nanostructured earth-abundant copper sulfides bulk materials. Adv. Energy Mater. **6**, 1600607 (2016)
41. P. Seo, S. Youn, C. Kang, The effect of test specimen size and strain-rate on liquid segregation in deformation behavior of mushy state material. J. Mater. Process. Technol. **130**, 551–557 (2002)
42. D. Mandrus, B. Sales, V. Keppens, B. Chakoumakos, P. Dai, L. Boatner, R. Williams, J. Thompson, T. Darling, A. Migliori, Filled skutterudite antimonides: validation of the electron-crystal phonon-glass approach to new thermoelectric materials. MRS Proc (1997). https://doi.org/10.1557/PROC-478-199
43. D. Voneshen, H. Walker, K. Refson, J. Goff, Hopping time scales and the phonon-liquid electron-crystal picture in thermoelectric copper selenide. Phys. Rev. Lett. **118**, 145901 (2017)
44. H. Liu, X. Shi, F. Xu, L. Zhang, W. Zhang, L. Chen, Q. Li, C. Uher, T. Day, G.J. Snyder, Copper ion liquid-like thermoelectrics. Nat. Mater. **11**, 422–425 (2012)
45. M. Tan, Y. Hao, Y. Deng, J. Chen, High thermoelectric properties of $(Sb, Bi)_2Te_3$ nanowire arrays by tilt-structure engineering. Appl. Surf. Sci. **443**, 11–17 (2018)
46. Y.-H. Zhao, Z.-H. Shan, W. Zhou, R. Zhang, J. Pei, H.-Z. Li, J.-F. Li, Z.-H. Ge, Y.-B. Wang, B.-P. Zhang, Enhanced thermoelectric performance of Bi–Se Co-doped $Cu_{1.8}S$ via carrier concentration regulation and multiscale phonon scattering. ACS Appl. Energy Mater (2022). https://doi.org/10.1021/acsaem.2c00414
47. Q. Hu, W. Qiu, L. Chen, J. Chen, L. Yang, J. Tang, Realize high thermoelectric properties in n-Type $Bi_2Te_{2.7}Se_{0.3}/Y_2O_3$ nanocomposites by constructing heterointerfaces. ACS Appl. Mater. Interfaces **13**, 38526–38533 (2021)
48. X. Lu, Q. Zhang, J. Liao, H. Chen, Y. Fan, J. Xing, S. Gu, J. Huang, J. Ma, J. Wang, High-efficiency thermoelectric power generation enabled by homogeneous incorporation of MXene in $(Bi, Sb)_2Te_3$ matrix. Adv. Energy Mater. **10**, 1902986 (2020)
49. R. Cao, E. Li, Q. Hu, Z. Zhu, Y. Zhang, X. Li, X. Hu, H. Song, Enhanced thermoelectric properties of $Cu_{2-\delta}Se$ nanopowder dispersed $Bi_2Ba_2Co_2O_y$ ceramics. Appl. Phys. A **124**, 669 (2018)
50. X. Liu, R. Cao, Y. Zhang, Z. Tian, X.-J. Li, H. Song, Excellent dispersion effects of carbon nanodots on the thermoelectric properties of $Bi_2Te_{2.7}Se_{0.3}$ with excessive Te. J. Alloys Compd. **899**, 163296 (2022)
51. M. Fan, Y. Zhang, X.-J. Li, H. Song, High thermoelectric performance in nano-SiC dispersed $Bi_{1.6}Pb_{0.4}Sr_2Co_2O_y$ compounds. J. Alloys Compd. **825**, 154065 (2020)